

Search for a direction in the forest of Lyman- α

Dhiraj Kumar Hazra,^a Arman Shafieloo^b

^aAsia Pacific Center for Theoretical Physics, Pohang, Gyeongbuk 790-784, Korea

^bKorea Astronomy and Space Science Institute 776, Daedeokdae-ro, Yuseong-gu, Daejeon 305-348, Korea

E-mail: dhiraj@apctp.org, shafieloo@kasi.re.kr

Abstract. We report the first test of isotropy of the Universe in the matter dominated epoch using the Lyman- α forest data from the high redshift quasars ($z > 2$) from SDSS-III BOSS-DR9 datasets. Using some specified data cuts, we obtain the probability distribution function (PDF) of the Lyman- α forest transmitted flux and use the statistical moments of the PDF to address the isotropy of the Universe. In an isotropic Universe one would expect the transmitted flux to have consistent statistical characteristics in different parts of the sky. We trisect the total survey area of 3275 deg² along the galactic latitude and using quadrant convention. We also make three subdivisions in the data for three different signal-to-noise-ratios (SNR). Finally we obtain and compare the statistical moments in the mean redshifts of 2.3, 2.6 and 2.9. We find, that the moments from all patches agree at all redshifts and at all SNRs, within 3σ uncertainties. Since Lyman- α transmitted flux directly maps the neutral hydrogen distribution in the inter galactic medium (IGM), our results indicate, within the limited survey area and sensitivity of the data, the distribution of the neutral hydrogen in the Universe is consistent with isotropic distribution. We should mention that we report few deviations from isotropy in the data with low statistical significance. Increase in survey area and larger amount of data are needed to make any strong conclusion about these deviations.

Contents

1	Introduction	1
2	Data analysis	2
2.1	Quasar selection, data cuts	2
2.2	Selection of sky patches	3
2.3	Error estimation	6
3	Analysis, results and discussions	6
4	Conclusions	12
5	Acknowledgments	12

1 Introduction

Our understanding of the physical cosmology strongly depends on the data that we observe and the model assumptions that we make. Assumptions in the standard model sometime pose problems in understanding the true nature of the Universe. Statistical isotropy is one of such assumptions which we assume in almost all the data analysis. In this assumption we claim that the statistical properties of the observables in the Universe are same in all direction. While in parameter estimations from the datasets, isotropy is assumed, there have been a number of tests to confirm this assumption, using data from different cosmological probes, such as Cosmic Microwave Background (CMB) [1–18] and Large Scale Structure (LSS) [19–30]. In this paper we investigate isotropy of the matter dominated Universe using the Lyman- α forest datasets in the redshift range $z \sim 2 - 3$. Spectra of high redshift quasars contain absorption lines that trace the components of the IGM along the line of sight. In the case of Lyman- α forest, we find absorption lines from the first ionization state of the Hydrogen atoms. The wavelength of the absorption identifies the redshift of the neutral hydrogen cloud. Analyzing these absorption lines, collectively from a number of quasars, we can constrain properties of the IGM. In particular, the Lyman- α transmitted flux (F) (absorption *w.r.t* the estimated continuum spectrum) can be related to the dark matter overdensity (δ) as $F = \bar{F} \exp[-A(1+\delta)^{2-0.7(\gamma-1)}]$ [31], where, \bar{F} is the mean transmitted flux, $\gamma - 1$ dictates the temperature density relation and A is a redshift dependent constant. We shall address the statistics of the transmitted flux in the Lyman- α region at different redshifts. To have a theoretical model independent analysis, in this work we only consider the statistical properties of the observational data. In the last decade, detection of large number of quasar spectrum with high SNR enables us to perform this type of analysis. We use Baryon Oscillation Spectroscopic Survey (BOSS) DR9 from Sloan Digital Sky Survey (SDSS)-III [32, 33]. We perform our test in three different redshifts in the matter dominated epoch that enables us to track the isotropy along time. In

each redshift, the isotropy is tested in medium, high and highest SNR of detection. We divide the sky in three patches using two different patch selection criteria. Since SDSS is a ground base survey which only has partial sky coverage, our test of isotropy will be limited by the survey area. Throughout the analysis we closely follow the survey parameters for the selection of data pixels from the quasar spectrum in order to obtain the PDF of the transmitted flux.

The paper is organized as follows : In section 2 we discuss the data from BOSS-DR9 and the selection criteria for the data pixels for our analysis. We also outline the error estimation procedure for the flux PDF. Afterwards we discuss and tabulate the properties of the sky patches selected. In the results section 3 we discuss the main outcome of our analysis. Finally in section 4 we conclude along with highlighting future prospects.

2 Data analysis

We use the latest available BOSS DR9 quasar Lyman- α forest data [34]. The ninth data release contains 54,468 spectra of Lyman- α quasars with redshifts more than 2.15. They provide Lyman- α forest data in the redshift range $z \sim 2 - 5.7$. However due to a smaller number of quasars with redshift higher than $z \sim 3$ we restrict our analysis in the redshift $z \sim 2 - 3$. BOSS-DR9 has a survey area of 3275 square degrees and hence our test of isotropy will be limited by this area. As has been discussed in [34], out of 87,822 total spectra, the set of 54,468 spectra was selected after removing low redshift quasars, quasars having broad absorption lines, too low SNR and negative continuum. Note that the continuum to each quasar spectrum is estimated using mean-flux regulated principal component analysis (MF-PCA) techniques [35] and they are provided along with the data. We would like to mention that even at this stage not all the data are appropriate for the isotropy test due to low SNR, damped Lyman- α (DLA), limited exposures and few other characteristics. Below we point out the data cuts that we have used to select a spectrum.

2.1 Quasar selection, data cuts

Our selection of data closely follows the BOSS criteria used to obtain constraints on the IGM [36]. As we mentioned earlier, we test the isotropy of the sky in three redshift bins with the central redshifts being 2.3, 2.6 and 2.9. The redshift bins have a bin width of $\Delta z = 0.3$. In each of the redshift bins we impose the following data cuts. Firstly since large number of low SNR quasars can have a systematic bias in our results, we reject all the quasars with $\text{SNR} < 6$. The rest of the quasars are binned in *good* ($6 \leq \text{SNR} < 8$), *better* ($8 \leq \text{SNR} < 10$) and *best* ($\text{SNR} \geq 10$) categories. In the quasar rest frame we use $1041 - 1185\text{\AA}$ as the Lyman- α domain.

Lyman- α forest typically refers to neutral hydrogen atoms with column density of 10^{14} atoms per cm^2 in the line of sight. The presence of DLA in a spectrum indicates extremely high column density ($\mathcal{O}(10^{20})$ atoms per cm^2). Following [36] we discard spectra with identified DLA in the sightlines. The provided data uses a DLA

concordance catalogue for the identification of DLA's. The detection efficiency of the catalogue decreases below neutral hydrogen column densities less than $10^{20.3}/\text{cm}^2$. Hence, below this criteria, in our analysis, for each of the forest we correct the flux for the damping wings of DLA in the sightlines, provided with the data [34]. We leave the spectra with neutral hydrogen column density of more than $10^{20.3}/\text{cm}^2$ out of our analysis.

As mentioned earlier, the survey provides the continuum of each spectrum estimated using MF-PCA technique. Note that the transmitted flux is the observed flux *w.r.t.* the estimated continuum and hence a bad continuum estimation shall bias the calculated flux *. Here too, following the survey criteria we reject the quasars which do not provide good fit to the spectrum redwards to the Lyman- α forest. We also reject spectra which had less than three individual exposures.

Our final selection criteria depends on the resolution of the BOSS spectographs. As has been mentioned in [36], BOSS spectographs do not resolve the Lyman- α forest. To evade this systematic effect that can reflect in the transmitted flux, we use similar procedure used in [36]. We stack the spectra according to the intrinsic wavelength dispersion (σ_{disp}) at the Lyman- α wavelength of each central redshift bin. Note that in each pixel the σ_{disp} is provided along with the spectrum. From each redshift bin we then discard the 5% spectra from below and 10% spectra from above.

Each quasar spectrum contain certain number of data pixels in the Lyman- α region. In a redshift bin (say, $2.15 < z < 2.45$) some quasars may have all the Lyman- α pixels, some will have partial pixels from either blue end or red end of the Lyman- α domain. We here consider all the quasars satisfying the above criteria and also contributing more than 30 pixels in the redshift window.

2.2 Selection of sky patches

Since BOSS-DR9 surveys in 3275 deg^2 area, we need to make patches in the sky in particular ways. First we convert the coordinate of the quasars from J2000 equatorial system to galactic coordinate (l, b) system. Below, in Fig. 1 we provide our selection of patches with different colors. In the first system we divide the sky using quadrant convention. Here we divide the sky in three patches where one patch remains in the southern hemisphere (red, $b < 0^\circ$) and the other two patches are in northern hemisphere ($b > 0^\circ$). The two patches in the northern hemisphere are divided in $l > 180^\circ$ (blue) and $l < 180^\circ$ (green) parts. In principle, the quadrant convention divides the southern hemisphere into two parts ($l > 180^\circ$ and $l < 180^\circ$) too, but since there are barely any data in $b < 0^\circ, l > 180^\circ$, we take only one patch from southern hemisphere. In our other selection, we divide the sky according to galactic latitude. The red patch remains same as it stays in the southern hemisphere. The patches in the northern hemisphere are divided in one patch with $b > 50^\circ$ (magenta) and another with $0^\circ < b \leq 50^\circ$ (black). Our first selection of patches is provided in the left of Fig. 1 and the other selection is shown to the right.

In the following table 1 we tabulate the essential information about the selected patches and the overall sample in different redshift and different SNR. For different

*The effects of different continuum estimations are discussed in [37]

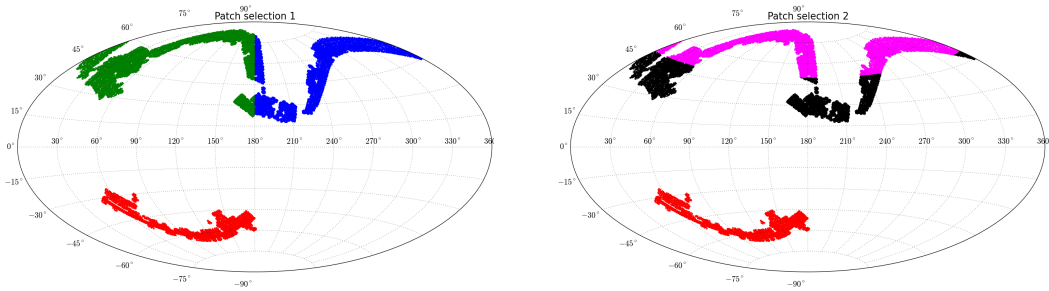


Figure 1. The BOSS-DR9 survey area in galactic coordinates and our selection of sky patches for the test of isotropy. To accommodate comparable number of quasars in each patch we have divided the sky in two manner, namely patch selection 1 (left) and patch selection 2 (right).

patches we provide the number of quasars and the number of pixels that pass all our data cuts discussed in the paragraph before. Note that apart from the red patch that stays in the southern hemisphere, other patches contain quasar number and the pixels that are comparable to each other. As we go towards higher redshifts we find lesser number of data pixels which is expected as we know there are not many high redshift quasars. This decrease in number of high redshift quasars limit our analysis to $z < 3$. However, in each SNR bin we have enough pixels to perform a relatively robust statistical analysis. Also note that compared to $6 \leq \text{SNR} < 8$ bin, in the two higher SNR bins the numbers of quasars or pixels are approximately half. We should mention that this is not a concern since we assume the data from different SNR are independent and we compare the statistical properties of the transmitted flux in each SNR separately. Moreover the lack of large number of quasars in higher SNR bins are compensated by the less dispersion in the data from higher SNR quasar samples.

Redshift range(z)	SNR	Patch location	Number of quasars	Number of Lyman- α pixels
2.15 – 2.45 ($\bar{z} = 2.3$)	6 – 8	Complete sky	1091	285878
		$b < 0^\circ$ (Red)	226	60631
		$b > 0^\circ, l < 180^\circ$ (Green)	390	100289
		$b > 0^\circ, l > 180^\circ$ (Blue)	475	124958
		$0^\circ < b < 50^\circ$ (Black)	401	106772
		$b > 50^\circ$ (Magenta)	464	118475
	8 – 10	Complete sky	498	130242
		$b < 0^\circ$ (Red)	106	28686
		$b > 0^\circ, l < 180^\circ$ (Green)	185	48158
		$b > 0^\circ, l > 180^\circ$ (Blue)	207	53398
		$0^\circ < b < 50^\circ$ (Black)	168	45290
		$b > 50^\circ$ (Magenta)	224	56266
	> 10	Complete sky	567	147679
		$b < 0^\circ$ (Red)	122	30899
		$b > 0^\circ, l < 180^\circ$ (Green)	187	47806
		$b > 0^\circ, l > 180^\circ$ (Blue)	258	68974
		$0^\circ < b < 50^\circ$ (Black)	228	62655
		$b > 50^\circ$ (Magenta)	217	54125
2.45 – 2.75 ($\bar{z} = 2.6$)	6 – 8	Complete sky	975	230165
		$b < 0^\circ$ (Red)	221	53062
		$b > 0^\circ, l < 180^\circ$ (Green)	373	86995
		$b > 0^\circ, l > 180^\circ$ (Blue)	381	90108
		$0^\circ < b < 50^\circ$ (Black)	348	80712
		$b > 50^\circ$ (Magenta)	406	96391
	8 – 10	Complete sky	475	107539
		$b < 0^\circ$ (Red)	110	25099
		$b > 0^\circ, l < 180^\circ$ (Green)	181	41564
		$b > 0^\circ, l > 180^\circ$ (Blue)	184	40876
		$0^\circ < b < 50^\circ$ (Black)	141	32220
		$b > 50^\circ$ (Magenta)	224	50220
	> 10	Complete sky	607	144797
		$b < 0^\circ$ (Red)	139	33690
		$b > 0^\circ, l < 180^\circ$ (Green)	224	54156
		$b > 0^\circ, l > 180^\circ$ (Blue)	244	56951
		$0^\circ < b < 50^\circ$ (Black)	248	56434
		$b > 50^\circ$ (Magenta)	220	54673
2.75 – 3.05 ($\bar{z} = 2.9$)	6 – 8	Complete sky	628	139373
		$b < 0^\circ$ (Red)	135	30291
		$b > 0^\circ, l < 180^\circ$ (Green)	250	57698
		$b > 0^\circ, l > 180^\circ$ (Blue)	243	51384
		$0^\circ < b < 50^\circ$ (Black)	225	50412
		$b > 50^\circ$ (Magenta)	268	58670
	8 – 10	Complete sky	372	87257
		$b < 0^\circ$ (Red)	75	17879
		$b > 0^\circ, l < 180^\circ$ (Green)	150	35068
		$b > 0^\circ, l > 180^\circ$ (Blue)	147	34310
		$0^\circ < b < 50^\circ$ (Black)	112	25351
		$b > 50^\circ$ (Magenta)	185	44027
	> 10	Complete sky	432	97826
		$b < 0^\circ$ (Red)	111	25645
		$b > 0^\circ, l < 180^\circ$ (Green)	174	37713
		$b > 0^\circ, l > 180^\circ$ (Blue)	147	34468
		$0^\circ < b < 50^\circ$ (Black)	164	39660
		$b > 50^\circ$ (Magenta)	157	32521

Table 1. The number of quasars and the number of Lyman- α pixels that contribute in different bins and patches. We bin our samples in three different redshift bins with mean redshift being 2.3, 2.6 and 2.9 and also in three signal-to-noise-ratio, namely $6 \leq \text{SNR} < 8$, $8 < \text{SNR} < 10$ and $\text{SNR} \geq 10$. The whole sky is divided in two different patch types (see, Fig. 1). Each type contains three different patches with different color codes provided in this table.

2.3 Error estimation

In this paper, as we have mentioned earlier, we compare the statistical properties of the observed data in different direction of the sky without comparing with any theoretical model. To obtain the uncertainties/errors in the estimated PDF of the transmitted flux, we need to generate the covariance matrix associated with the flux PDF. Here too, we follow similar procedure as adopted in the BOSS analysis, in order to obtain the covariance matrix. We follow bootstrap resampling of the data in each bin. We have a total of 36 bins in both type of patch selection: 3 SNR bins, 3 redshift bins and 4 bins corresponding to each of the 3 patches and a complete sample. In each bin, we gather all the pixels that pass through our data cut and provided in Table 1. We perform bootstrap resampling of chunks upto 100\AA wavelengths obtained from each quasar spectrum and generate 1000 realizations of the data. From these samples covariance matrix of the flux PDF can be easily calculated. Using different realizations we did check the convergence of the diagonal terms of the covariance matrix and we could conclude that the choice of 1000 realizations has been conservative.

We concentrate on the statistical properties of the PDF or the data. Hence we calculate different statistical moments such as mean, median, variance, skewness and kurtosis of the PDF. We report the moments of the distribution that we obtain from the original data as well as the upper and lower error bounds on each of the moments that we calculate from the bootstrap simulations. For distribution of each moment, we generate the empirical cumulative distribution function (ECDF) and report the (34.15%) upper and lower error bounds, which we hereafter shall refer as 1σ uncertainties in the distribution of the particular moment.

Before discussing the isotropy test on patches in next section, in Table 2 we report the mean transmitted flux and 1σ uncertainties of the flux PDF that we obtain from the complete sample in the three redshifts and in three SNR bins. The number of quasars and the number of pixels that are used in our analysis are provided in Table 1 for the complete sample size. Note that as we go back in time (higher in redshift) the increase of neutral hydrogen is evident from the decrease of the transmitted flux in all SNR. In each SNR, the error on the flux are comparable and that indicates, though at high SNR the signal is better, the less number of quasars in high SNR keeps the uncertainties comparable to the uncertainties at lower SNR which contain larger number of quasars (for example, compare the *good* and the *best* SNR cases).

3 Analysis, results and discussions

In the previous section we mentioned that we trisect the survey area in two ways. One patch, that is in southern galactic hemisphere remains common to both the selection. For the 5 patches, that are color coded (red, green, blue, magenta and black) we obtain the PDF of transmitted flux. However, we compare the statistical properties of the PDF within each selection type.

To start with, we provide the flux PDF with the errors in Fig. 2 for patch selection 1 (corresponding to the selection in the left of Fig. 1) and in Fig. 3 for patch selection

Redshift range(z)	SNR	$\bar{F} \pm \Delta F$
2.15 – 2.45 ($\bar{z} = 2.3$)	6 – 8	$0.826^{+0.154}_{-0.375}$
	8 – 10	$0.822^{+0.138}_{-0.405}$
	> 10	$0.819^{+0.129}_{-0.487}$
2.45 – 2.75 ($\bar{z} = 2.6$)	6 – 8	$0.762^{+0.172}_{-0.39}$
	8 – 10	$0.758^{+0.159}_{-0.427}$
	> 10	$0.756^{+0.152}_{-0.454}$
2.75 – 3.05 ($\bar{z} = 2.9$)	6 – 8	$0.69^{+0.191}_{-0.377}$
	8 – 10	$0.687^{+0.181}_{-0.396}$
	> 10	$0.686^{+0.176}_{-0.413}$

Table 2. The flux statistics of the Lyman- α forest transmitted flux in different redshift bins and different signal-to-noise bins, provided for the samples across the complete sky. The mean flux and the 1σ error bars on the PDF on both sides of the mean are provided.

2 (the right selection in the Fig. 1). The colors of the PDF's correspond to different patches (as shown in the Fig. 1). The PDF's are calculated in the flux range $[-0.2-1.5]$ in 34 bins. Theoretically the transmitted flux should be within 0 and 1 (for the complete and no absorption respectively) but due to the noise in observations and the bias in the continuum estimations, the transmitted flux might be obtained outside the theoretical boundary. The PDF's are normalized such that the total area under each PDF is 1. In both the figures, we provide the PDF for different redshifts and different SNR. As we mentioned in the previous section, due to less number of quasars in the higher SNR bins, the errors on the flux PDFs are comparable to that of the lower SNR bins. In the plots of the PDF, the difference between the PDF's in *good*, *better* and *best* SNR bins are evident. For the higher SNR bins the flux PDF are more sharp around the peak. It is interesting to note that at the same SNR and at the same redshift, the PDF of transmitted flux from different patches are very similar. In some of the bins we find the flux from one patch is different from other ones. To quantify the difference, we next look for the different moments of the PDFs.

In this paper, we restrict ourselves to calculating up-to the fourth moment, *i.e.* till kurtosis of the PDF. We calculate the mean (\bar{F}), the median ($F_{1/2}$), the variance (σ^2), the skewness (s) and the kurtosis (κ) of the flux PDFs in each bin. Since we have noticed in Fig. 2 and 3 that the PDFs are very different in different redshifts, we report the residual of such quantities obtained in a patch *w.r.t.* the complete sample. In Fig. 4 we plot the 5 statistical quantities in residual space for the patch selection 1 and in Fig. 5 we plot the same quantities for patch selection 2. As we are plotting in residual space, we find the moments are distributed about the zero. We should mention that here the errors represent the uncertainties of the corresponding statistical moments obtained from the ECDFs of the moments. The plotted errors represent 1σ uncertainties.

Note that almost all the statistical moments from different patches are comparable

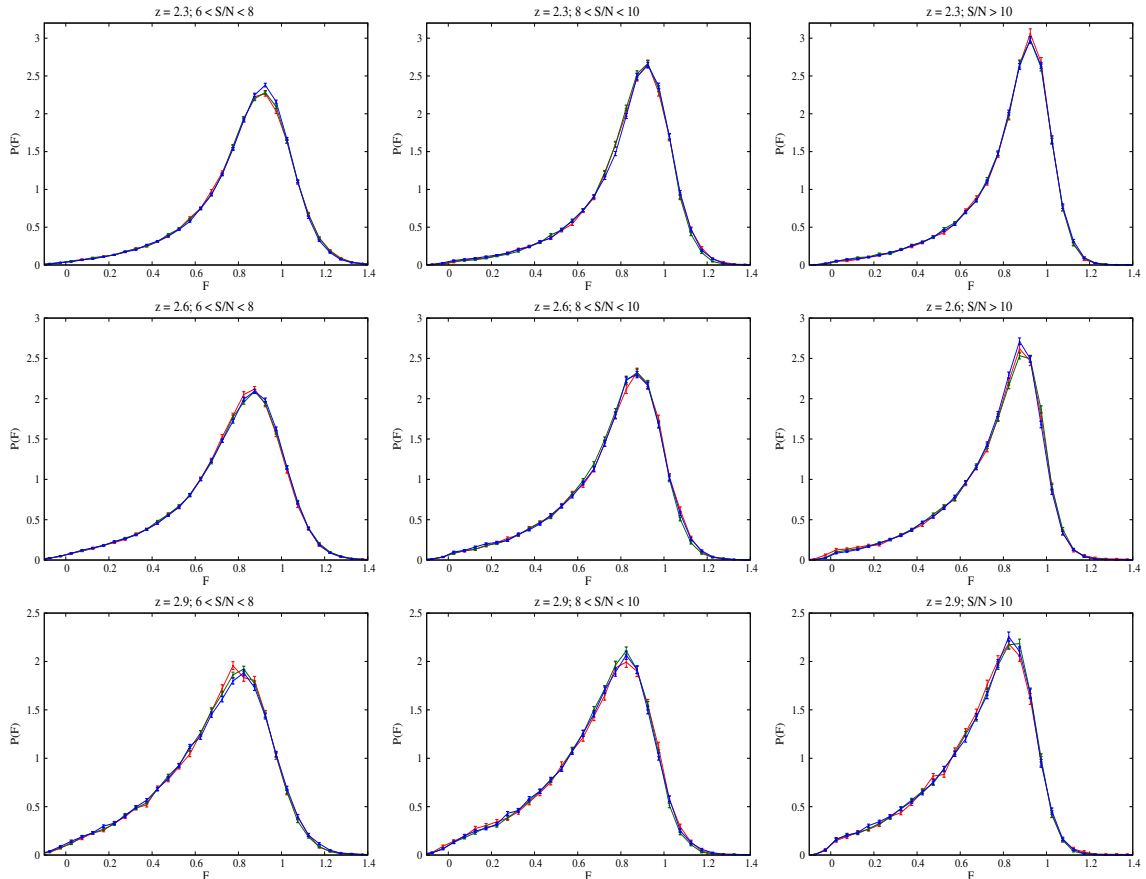


Figure 2. Comparison of PDF of the Lyman- α transmitted flux in different patches for patch selection 1 (left of Fig. 1). The color codes represent the PDF's from the corresponding patches. Along the rows we plot PDF's for different redshifts and along the columns we plot for different SNR. The error on the PDF is estimated through bootstrap resampling over 100Å data chunks.

to each other within their associated uncertainties. We would like to stress that we find this consistency throughout redshift 2 – 3 and at all SNRs. Hence our results are *consistent with the isotropic distribution of neutral hydrogen* and also *consistent with isotropic absorption of photons by the hydrogen clouds in the IGM at different redshifts*.

A closer examination shows that almost none of the patches contain any moment which is systematically higher/lower than the total sample during the time evolution. Hence the properties in each patch is preserved during the matter dominated expansion of the Universe.

We should mention that we have obtained some deviations from isotropy in our analysis. We find the residual moments for the blue patch and the red patch (for patch selection 1) do not agree at 2σ level in cases. For example, we refer to the median mismatch (at $z = 2.3$, $6 \leq \text{SNR} < 8$), the variance mismatches (at $z = 2.9$, $6 \leq \text{SNR} < 8$ and at $z = 2.6$, $\text{SNR} \geq 10$) and skewness mismatches (at $z = 2.9$ at $8 \leq \text{SNR} < 10$). Similarly, for patch selection 2 we find such deviations at 2σ level within the red and the black patches. Since, the number of such deviations are only a

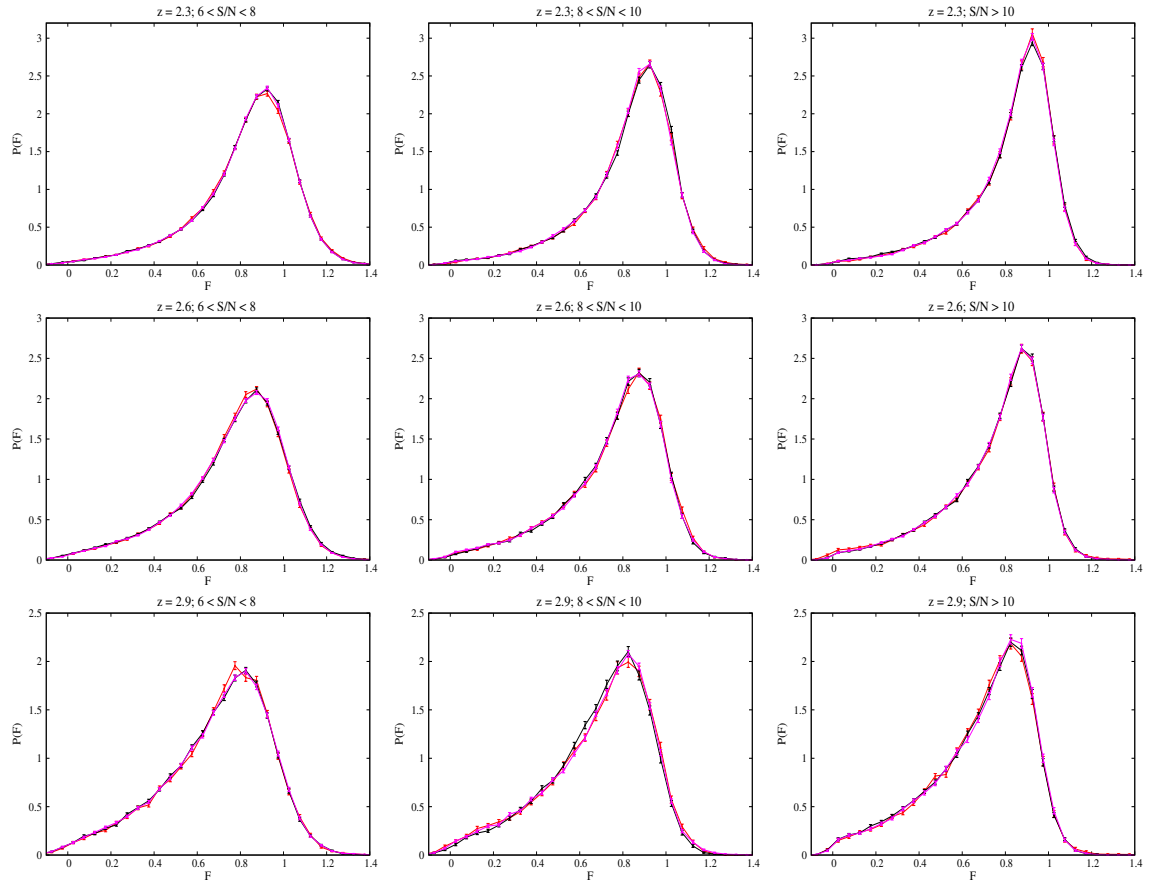


Figure 3. Comparison of PDF of the Lyman- α transmitted flux in different patches for patch selection 2 (right of Fig. 1). The color codes represent the PDF's from the corresponding patches. Along the rows we plot PDF's for different redshifts and along the columns we plot for different SNR. The error on the PDF is estimated through bootstrap resampling over 100Å data chunks.

few and all the moments agree within 3σ , we do not report any statistically significant deviation. Moreover, we should note that due to less number of quasars, the red patch at the southern hemisphere contains the largest dispersion in the distribution of the statistical moments which in turn can lead to such fluctuations. Hence, in order to rule out or confirm any deviations between the blue and the red patches (or between black and red patches) we need more detection of Lyman- α forest in the southern galactic hemisphere. Future surveys will be able to provide significantly more quasar spectra with higher sky coverage, which are essential to extend this initiative beyond the flux PDF level.

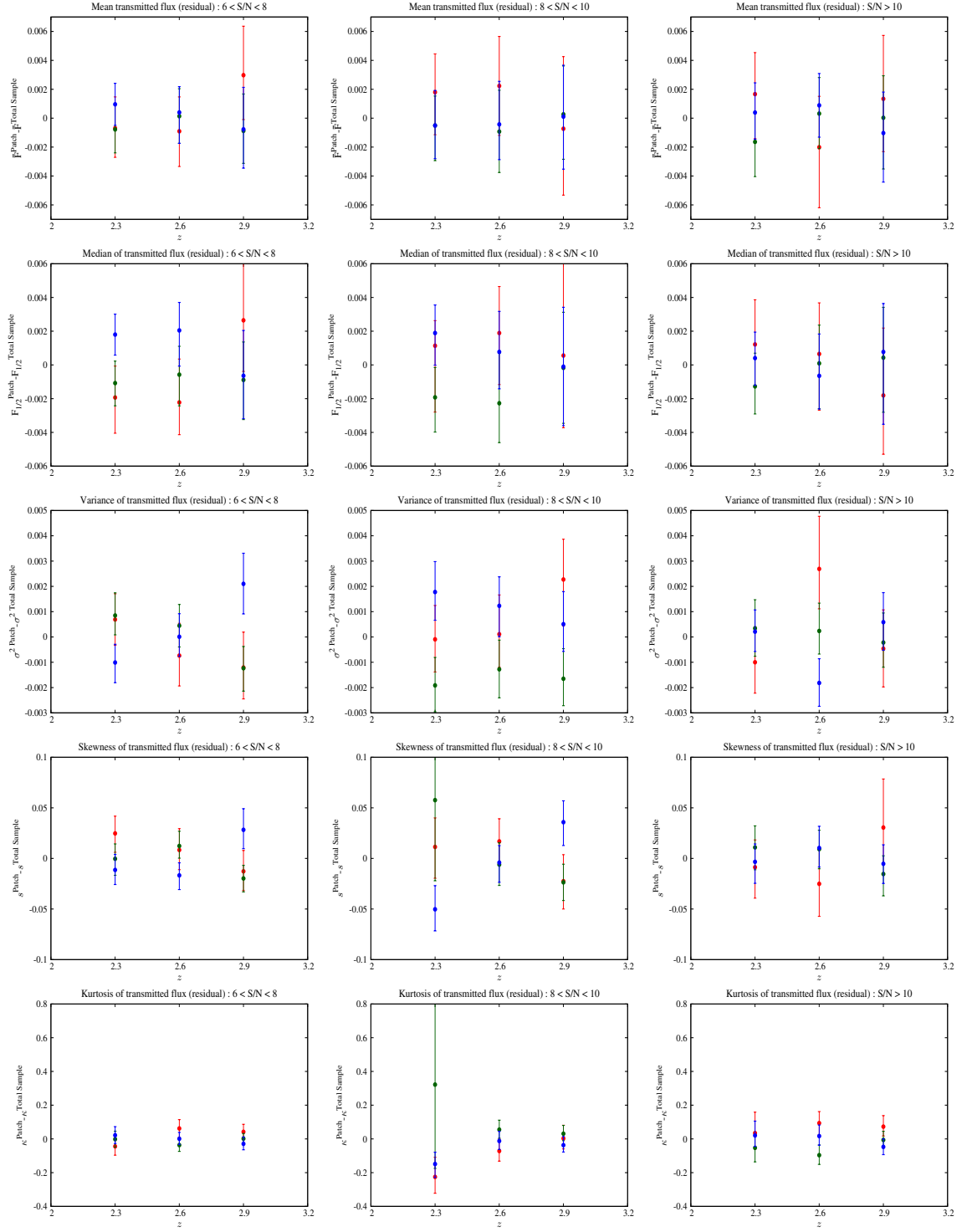


Figure 4. First few statistical moments of the Lyman- α transmitted flux PDF for different parts of the sky. For relative comparison we plot the residual moments from the total sample. The error bars correspond to the 1σ bounds on that particular moment. This figure represents the comparison between the properties of the patches for patch selection 1 (left plot of Fig. 1).

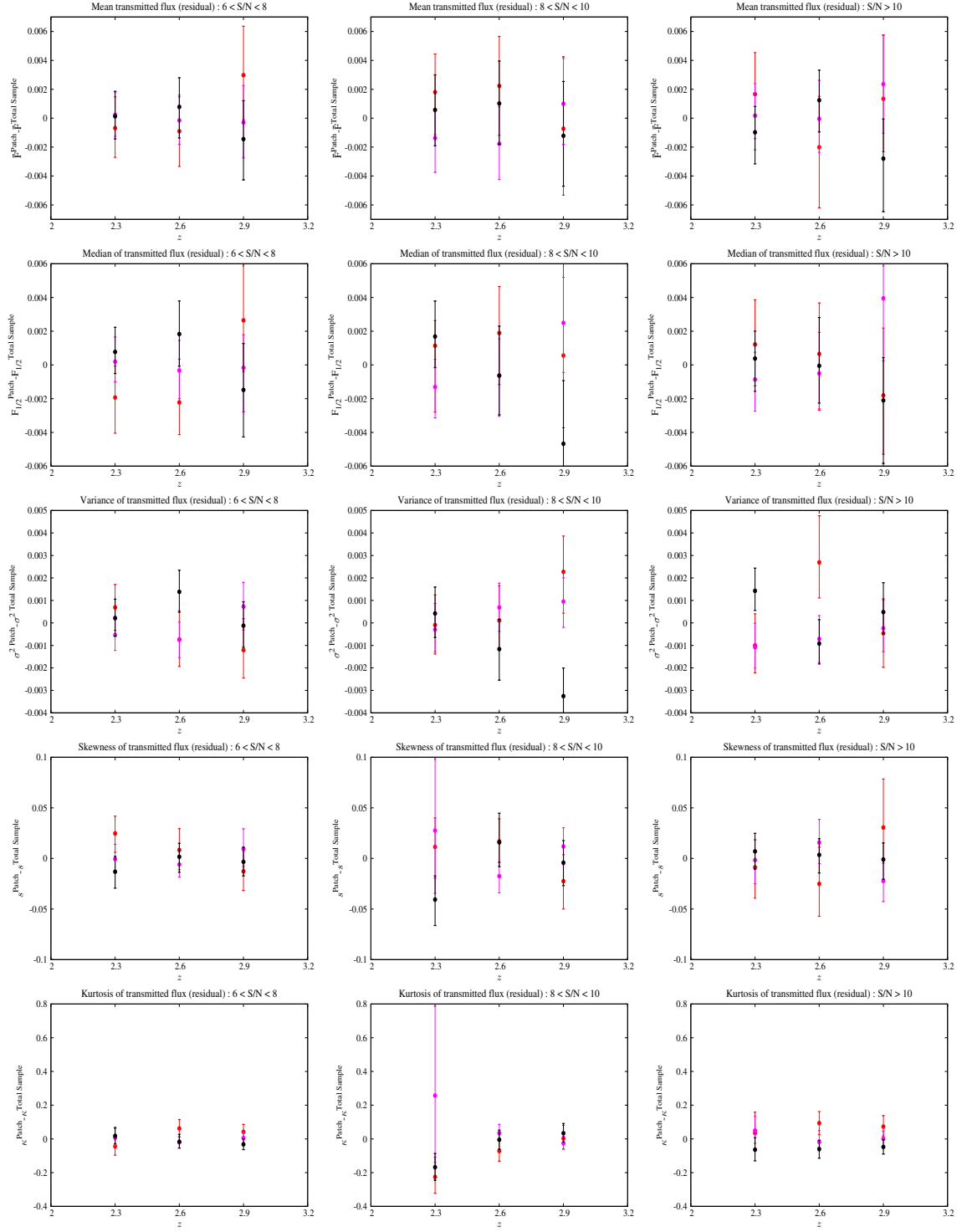


Figure 5. First few statistical moments of the Lyman- α transmitted flux PDF for different parts of the sky. For relative comparison we plot the residual moments from the total sample. The error bars correspond to the 1σ bounds on that particular moment. This figure represents the comparison between the properties of the patches for patch selection 2 (right plot of Fig. 1).

4 Conclusions

As a first approach to test the isotropy in the matter dominated epoch we have used the Lyman- α forest data in this paper. In order to remain independent from theoretical assumptions of the IGM, we have used only the observational data and compared the statistical properties of the PDF of the observed flux in different directions of the sky. Detection of large number high redshift quasar spectra by BOSS has enabled us to perform this test. Though we report the distribution of neutral hydrogen is consistent with isotropic Universe during $z \sim 2-3$, making any general claim about the isotropy of the Universe requires much more sky coverage. As we have mentioned before, our test of anisotropy is *partial* due to only 3275 deg^2 sky coverage. With a larger sky coverage we can address the precise direction and significance of the possible anisotropy, if present. With upcoming observations like e-BOSS [38] and DESI [39] we expect to detect higher quality of Lyman- α forest data, significantly higher number of quasar spectra with larger sky coverage. Hence, with the upcoming data the assumption of isotropy can be falsified with higher precision. Cross-correlating the data from different surveys will be also important to rule out any systematic effect.

Any presence of anisotropy in the Lyman- α forest is interesting and it points towards the distribution of neutral hydrogen, temperature-density relation and few other properties in the IGM. A straightforward extension of this topic would be to model the IGM using some semi-analytical modeling or simulations. With the modeling we can address if the significance of such anisotropy being statistical or physical. Moreover, if any physical anisotropy is found, we need to examine the change in the properties of the IGM it refers to and search for the probable cause.

We would like to conclude by mentioning that the major finding of our analysis is *consistency of the data with the isotropic Universe in the final stage of matter dominated epoch ($z \sim 2-3$), and unfortunately we found no preferred direction in the Lyman- α forest to guide the travelers*. Though our result is a partial test, if similar tests on larger survey area also confirms the isotropy, that might hint towards the possibility that any late time anisotropy is probably caused by bulk flow and not an intrinsic anisotropy in the Universe.

5 Acknowledgments

We would like to thank Tapomoy Guha Sarkar for important discussions, suggestions and comments on the manuscripts. We would also like to thank Amir Aghamousa, Stephen Appleby, Eric Linder, Pat McDonald, Graziano Rossi and Tirthankar Roy Choudhury for their comments and suggestions. We thank Khee-Gan Lee for various clarifications regarding the BOSS analysis of the Lyman- α forest data. D.K.H. wish to acknowledge support from the Korea Ministry of Education, Science and Technology, Gyeongsangbuk-Do and Pohang City for Independent Junior Research Groups at the Asia Pacific Center for Theoretical Physics. A.S. would like to acknowledge the support of the National Research Foundation of Korea (NRF-2013R1A1A2013795). We acknowledge the use of data from SDSS III. Funding for SDSS-III has been provided

by the Alfred P. Sloan Foundation, the Participating Institutions, the National Science Foundation, and the U.S. Department of Energy Office of Science. The SDSS-III web site is <http://www.sdss3.org/>.

SDSS-III is managed by the Astrophysical Research Consortium for the Participating Institutions of the SDSS-III Collaboration including the University of Arizona, the Brazilian Participation Group, Brookhaven National Laboratory, Carnegie Mellon University, University of Florida, the French Participation Group, the German Participation Group, Harvard University, the Instituto de Astrofísica de Canarias, the Michigan State/Notre Dame/JINA Participation Group, Johns Hopkins University, Lawrence Berkeley National Laboratory, Max Planck Institute for Astrophysics, Max Planck Institute for Extraterrestrial Physics, New Mexico State University, New York University, Ohio State University, Pennsylvania State University, University of Portsmouth, Princeton University, the Spanish Participation Group, University of Tokyo, University of Utah, Vanderbilt University, University of Virginia, University of Washington, and Yale University.

References

- [1] G. Hinshaw, A. J. Banday, C. L. Bennett, K. M. Gorski, A. Kogut, C. H. Lineweaver, G. F. Smoot and E. L. Wright, *Astrophys. J.* **464** (1996) L25 [astro-ph/9601061].
- [2] D. N. Spergel *et al.* [WMAP Collaboration], *Astrophys. J. Suppl.* **148** (2003) 175 [astro-ph/0302209].
- [3] C. J. Copi, D. Huterer, D. J. Schwarz and G. D. Starkman, *Adv. Astron.* **2010** (2010) 847541 [arXiv:1004.5602 [astro-ph.CO]].
- [4] A. de Oliveira-Costa, M. Tegmark, M. Zaldarriaga and A. Hamilton, *Phys. Rev. D* **69** (2004) 063516 [astro-ph/0307282].
- [5] L. R. Abramo, A. Bernui, I. S. Ferreira, T. Villela and C. A. Wuensche, *Phys. Rev. D* **74** (2006) 063506 [astro-ph/0604346].
- [6] K. Land and J. Magueijo, *Phys. Rev. Lett.* **95** (2005) 071301 [astro-ph/0502237].
- [7] K. Land and J. Magueijo, *Mon. Not. Roy. Astron. Soc.* **378** (2007) 153 [astro-ph/0611518].
- [8] A. Rakic and D. J. Schwarz, *Phys. Rev. D* **75** (2007) 103002 [astro-ph/0703266].
- [9] P. K. Samal, R. Saha, P. Jain and J. P. Ralston, *Mon. Not. Roy. Astron. Soc.* **385** (2008) 1718 [arXiv:0708.2816 [astro-ph]].
- [10] P. K. Samal, R. Saha, P. Jain and J. P. Ralston, *Mon. Not. Roy. Astron. Soc.* **396** (2009) 511 [arXiv:0811.1639 [astro-ph]].
- [11] H. K. Eriksen, A. J. Banday, K. M. Gorski, F. K. Hansen and P. B. Lilje, *Astrophys. J.* **660** (2007) L81 [astro-ph/0701089].
- [12] J. Hoftuft, H. K. Eriksen, A. J. Banday, K. M. Gorski, F. K. Hansen and P. B. Lilje, *Astrophys. J.* **699** (2009) 985 [arXiv:0903.1229 [astro-ph.CO]].

- [13] C. Copi, D. Huterer, D. Schwarz and G. Starkman, Phys. Rev. D **75** (2007) 023507 [astro-ph/0605135].
- [14] C. J. Copi, D. Huterer, D. J. Schwarz and G. D. Starkman, Mon. Not. Roy. Astron. Soc. **367** (2006) 79 [astro-ph/0508047].
- [15] D. J. Schwarz, G. D. Starkman, D. Huterer and C. J. Copi, Phys. Rev. Lett. **93** (2004) 221301 [astro-ph/0403353].
- [16] T. Souradeep, A. Hajian and S. Basak, New Astron. Rev. **50** (2006) 889 [astro-ph/0607577].
- [17] P. A. R. Ade *et al.* [Planck Collaboration], arXiv:1303.5083 [astro-ph.CO].
- [18] Y. Akrami, Y. Fantaye, A. Shafieloo, H. K. Eriksen, F. K. Hansen, A. J. Banday and K. M. Grski, Astrophys. J. **784** (2014) L42 [arXiv:1402.0870 [astro-ph.CO]].
- [19] R. Fernandez-Cobos, P. Vielva, D. Pietrobon, A. Balbi, E. Martinez-Gonzalez and R. B. Barreiro, Mon. Not. Roy. Astron. Soc. **441** (2014) 2392 [arXiv:1312.0275 [astro-ph.CO]].
- [20] R. G. Cai, Y. Z. Ma, B. Tang and Z. L. Tuo, Phys. Rev. D **87** (2013) 12, 123522 [arXiv:1303.0961 [astro-ph.CO]].
- [21] R. C. Keenan, L. Trouille, A. J. Barger, L. L. Cowie and W. -H. Wang, Astrophys. J. Suppl. **186**, 94 (2010) [arXiv:0912.3090 [astro-ph.CO]].
- [22] R. C. Keenan, A. J. Barger, L. L. Cowie, W. -H. Wang, I. Wold and L. Trouille, Astrophys. J. **754** (2012) 131 [arXiv:1207.1588 [astro-ph.CO]].
- [23] R. C. Keenan, A. J. Barger and L. L. Cowie, Astrophys. J. **775** (2013) 62 [arXiv:1304.2884 [astro-ph.CO]].
- [24] J. R. Whitbourn and T. Shanks, arXiv:1307.4405 [astro-ph.CO].
- [25] W. J. Frith, G. S. Buswell, R. Fong, N. Metcalfe and T. Shanks, Mon. Not. Roy. Astron. Soc. **345** (2003) 1049 [astro-ph/0302331].
- [26] G. S. Buswell, T. Shanks, P. J. Outram, W. J. Frith, N. Metcalfe and R. Fong, [astro-ph/0302330].
- [27] W. J. Frith, P. J. Outram and T. Shanks, Mon. Not. Roy. Astron. Soc. **364** (2005) 593 [astro-ph/0507215].
- [28] W. J. Frith, T. Shanks and P. J. Outram, Mon. Not. Roy. Astron. Soc. **361** (2005) 701 [astro-ph/0411204].
- [29] W. J. Frith, P. J. Outram and T. Shanks, [astro-ph/0408011].
- [30] S. Appleby and A. Shafieloo, JCAP **1410**, no. 10, 070 (2014) [arXiv:1405.4595 [astro-ph.CO]].
- [31] L. Hui and N. Y. Gnedin, Mon. Not. Roy. Astron. Soc. **292**, 27 (1997) [astro-ph/9612232]; N. Y. Gnedin and L. Hui, Mon. Not. Roy. Astron. Soc. **296**, 44 (1998) [astro-ph/9706219, astro-ph/9706219]; P. McDonald, J. Miralda-Escude, M. Rauch, W. L. W. Sargent, T. A. Barlow and R. Cen, Astrophys. J. **562**, 52 (2001) [Astrophys. J. **598**, 712 (2003)] [astro-ph/0005553].
- [32] See, <http://www.sdss3.org/>

- [33] See, <https://www.sdss3.org/surveys/boss.php>
- [34] K. G. Lee, S. Bailey, L. E. Bartsch, W. Carithers, K. S. Dawson, D. Kirkby, B. Lundgren and D. Margala *et al.*, arXiv:1211.5146 [astro-ph.CO].
- [35] K. G. Lee, N. Suzuki and D. N. Spergel, *Astron. J.* **143**, 51 (2012) [arXiv:1108.6080 [astro-ph.CO]].
- [36] K. G. Lee, J. P. Hennawi, D. N. Spergel, D. H. Weinberg, D. W. Hogg, M. Viel, J. S. Bolton and S. Bailey *et al.*, *Astrophys. J.* **799**, no. 2, 196 (2015) [arXiv:1405.1072 [astro-ph.CO]].
- [37] N. G. Busca, T. Delubac, J. Rich, S. Bailey, A. Font-Ribera, D. Kirkby, J. M. Le Goff and M. M. Pieri *et al.*, *Astron. Astrophys.* **552**, A96 (2013) [arXiv:1211.2616 [astro-ph.CO]].
- [38] See, <https://www.sdss3.org/future/eboss.php>
- [39] See, <http://desi.lbl.gov>